Nucleotide-Dependent Conformational Changes in HisP: Molecular Dynamics Simulations of an ABC Transporter Nucleotide-Binding Domain

Jeff D. Campbell,*‡ Sundeep Singh Deol,* Frances M. Ashcroft,‡ Ian D. Kerr,† and Mark S. P. Sansom*
*Department of Biochemistry, University of Oxford, Oxford OX1 3QU, United Kingdom; †School of Biomedical Sciences, University of Nottingham, Queen's Medical Centre, Nottingham NG7 2UH, United Kingdom; and ‡University Laboratory of Physiology, University of Oxford, Oxford OX1 3PT, United Kingdom.

ABSTRACT ATP-binding cassette (ABC) transporters mediate the movement of molecules across cell membranes in both prokaryotes and eukaryotes. In ABC transporters, solute translocation occurs after ATP is either bound or hydrolyzed at the intracellular nucleotide-binding domains (NBDs). Molecular dynamics (MD) simulations have been employed to study the interactions of nucleotide with NBD. The results of extended (~20 ns) MD simulations of HisP (total simulation time ~80 ns), the NBD of the histidine transporter $HisQMP_2J$ from *Salmonella typhimurium,* are presented. Analysis of the MD trajectories reveals conformational changes within HisP that are dependent on the presence of ATP in the binding pocket of the protein, and are sensitive to the presence/absence of Mg ions bound to the ATP. These changes are predominantly confined to the α-helical subdomain of HisP. Specifically there is a rotation of three α-helices within the subdomain, and a movement of the signature sequence toward the bound nucleotide. In addition, there is considerable conformational flexibility in a conserved glutamine-containing loop, which is situated at the interface between the α-helical subdomain and the F1-like subdomain. These results support the mechanism for ATP-induced conformational transitions derived from the crystal structures of other NBDs.

INTRODUCTION

Members of the ATP-binding cassette (ABC) transporter family of proteins mediate a diverse spectrum of physiological processes ranging from nutrient uptake and toxin efflux in prokaryotes, to antigen presentation and bile salt export in eukaryotes (Higgins, 1992; Kerr, 2002; Jones and George, 2004). Overexpression, deletions, or mutations in mammalian ABC transporters lead to (or prevent pharmaceutical treatment of) diseases including cystic fibrosis, diabetes, and cancer.

ABC transporters comprise two transmembrane domains (TMDs) that form a pathway for allocrite (i.e., solute) transport across the membrane, and two cytoplasmic, nucleotide-binding domains (NBDs) (Fig. 1 *A*), which couple the energy of nucleotide binding and hydrolysis to allocrite transport. Many ABC transporters possess additional domains that either recruit allocrite (e.g., HisJ, the periplasmic binding protein of the histidine transport complex $HisQMP_2J$; Fig. 1 *A*) or function as regulatory domains. The NBDs exhibit a high degree of sequence and structure conservation across the transporter family and contain a number of conserved sequence motifs (Holland and Blight, 1999; Linton and Higgins, 1998). These include the Walker-A (W_A) and Walker-B (W_B) motifs (Walker et al., 1982), an ABC transporter-specific or ''signature'' motif (Fig. 1 *B*), and two shorter sequences containing conserved glutamine and histidine residues (Gln-loop and His-loop, respectively; Linton and Higgins, 1998). Recent crystallographic and biochemical (Fetsch and Davidson, 2002; Smith et al., 2002; Loo et al., 2002; Chen et al., 2003) studies have shown that the topology of the dimer formed by the two NBDs is also conserved.

Elucidation of the mechanism of ABC transporters requires not only determination of the (static) structures of the component domains (Hung et al., 1998; Smith et al., 2002; Chang and Roth, 2001; Chang, 2003; Locher et al., 2002), but also a detailed understanding of the conformational changes that occur to elicit transport (Linton and Higgins, 2002). Such conformational changes may occur both within a domain (in response to binding of nucleotide, for example) and between domains (allosteric interactions). Evidence has accrued that the initial event in the catalytic/transport cycle, namely the binding of nucleotide, is sufficient to induce a substantial conformational change. For example, in the human multidrug transporter P-glycoprotein (P-gp), binding of nucleotide is associated with allosteric changes that can be detected by altered immunoreactivity (Mechetner et al., 1997; Druley et al., 2001), pharmacologically (Martin et al., 2000), and structurally (Rosenberg et al., 2001; Sonveaux et al., 1999). Similarly, in the prokaryotic histidine importer the binding of nucleotide-induced changes in the structure of the NBD subunit (HisP) can be detected by altered reactivity of endogenous cysteines to maleimides (Kreimer et al., 2000), whereas in the maltose importer an altered structure in response to nucleotide binding has been observed (Schneider et al., 1994). Comparable results have been obtained for numerous other ABC transporters (Sharom, 2003).

Submitted June 1, 2004, and accepted for publication September 9, 2004.

Address reprint requests to Mark S. P. Sansom, Tel.: 44-1865-275371; Fax: 44-1865-275182; E-mail: mark.sansom@biop.ox.ac.uk.

0006-3495/04/12/3703/13 $2.00

doi: 10.1529/biophysj.104.046870

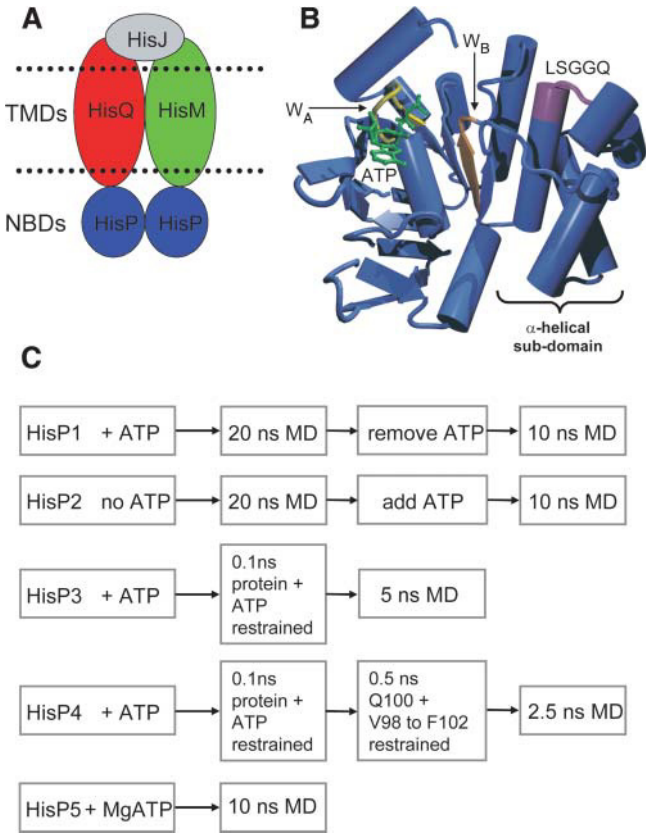

FIGURE 1 Structure of HisP and simulation protocols. (*A*) The domain organization of an ABC transporter is illustrated for the $HisQMP_2J$ complex. HisP is the intracellular NBD, HisQ, and HisM are the TMDs, and HisJ is a periplasmic binding protein. (*B*) The structure of the HisP monomer (PDB code 1BOU) is shown, indicating the conserved motifs (*yellow* is the Walker-A motif, W_A; *brown* is the Walker-B motif, W_B; and *purple* is the ''signature'' motif (LSGGQ). (*C*) Outline of the four simulations, HisP1–HisP5. (*HisP1*) In the first stage the water molecules present in the crystal structure and the ATP molecule were retained. The simulation system was prepared by solvation with ~10,000 SPC water molecules along with counterions to give electroneutrality plus randomly placed Na^+ and Cl^- ions equivalent to 0.1 M NaCl. This was followed by energy minimization. After 20 ns of MD, in the third stage, the ATP, water molecules, and ions were removed. System preparation followed by energy minimization was then repeated as described above. (*HisP2*) In the first stage the water molecules present in the crystal structure were retained but the ATP was removed. System preparation followed by energy minimization was as for HisP1. In the third stage the water molecules and ions were removed. ATP was added back to the system (by least-squares fitting to the W_A motif and conserved tyrosine Y16 in the original ATP-bound PDB and extracting the coordinates for ATP), and then system preparation followed by energy minimization was repeated. A short period (0.2 ns) of restrained MD was performed during which the W_A motif and Y16 residue were restrained followed by a further 0.2 ns during which the ATP was restrained, followed by a final stage of 10 ns unrestrained MD simulation. (*HisP3*) The first stage was as for HisP1. This was followed by a short (0.1 ns) period of restrained MD during which the protein (nonhydrogen atoms) and the ATP were restrained. There followed 5 ns of unrestrained MD simulation. (*HisP4*) The first and second stages were as for HisP3. The third stage consisted of 0.5 ns of MD during which the Q100 side chain and the backbone atoms of V98–F102 were restrained. There followed 2.4 ns of unrestrained MD simulation. (*HisP5*) Water molecules and ATP present in the crystal structure were retained but additionally a magnesium ion was added to the system by least-squares fitting to NaATP molecule in the MJ0796 dimeric structure (see Methods) (Smith et al., 2002). System preparation followed by energy minimization was as for HisP1. Ten nanoseconds of unrestrained MD was run on the minimized system.

A detailed understanding of the conformational changes elicited by the initial nucleotide-binding event is essential to elucidating the mechanism(s) of allosteric communication within the catalytic cycle of ABC transporters. Analyzing this early event in isolation is made possible by studies of prokaryotic ABC import systems, in which the NBDs are frequently expressed as isolated domains (Linton and Higgins, 1998). In many cases these NBDs have been expressed as soluble proteins and have been characterized in terms of their ability to bind and hydrolyze nucleotide with comparable activities to intact transporters (Nikaido and Ames, 1999; Morbach et al., 1993; Davidson et al., 1996). Furthermore, the structures of a number of such NBDs are available confirming the stability of the isolated domain or subunit (Hung et al., 1998; Diederichs et al., 2000). These studies identify three subdomains, namely an F1-like subdomain, a β-sheet specific subdomain and an α-helical subdomain (residues 109–171 in HisP) (Yuan et al., 2001; Karpowich et al., 2001). Understanding the conformational changes in isolated NBDs that result from binding of nucleotide is an essential first step toward understanding the more complex changes in the intact ABC transporter.

Although the crystal structures of ABC transporter NBDs are available, they present a static (time- and space-averaged) snapshots of the structure either in the presence or absence of bound nucleotide. A clearer understanding of conformational change requires elucidation of the dynamic structural changes occurring in response to nucleotide binding and hydrolysis. In this respect molecular dynamics (MD) simulations provide a tool for computational investigations of protein conformational changes. For example, MD has been used to demonstrate the conformational change in the prion protein due a mutation related to Gerstmann-Straussler-Sheinker disease (Okimoto et al., 2002), to study the structural changes in the F1 domain of the F1-ATPase (Bockmann and Grubmuller, 2002), to identify key residues in the myosin ATP hydrolysis cycle (Okimoto et al., 2001), to identify important ATP-binding residues in Wilson's disease protein (Efremov et al., 2004), and to explore changes in conformational dynamics related to ligand binding in, e.g., glutamate receptors (Arinaminpathy et al., 2002), periplasmic binding proteins (Pang et al., 2003), and transferrin (Rinaldo and Field, 2003).

In this study we report extended simulations of the NBD of the histidine transport system (HisP; Higgins et al., 1982). HisP is ideal for a MD study because it remains the highest resolution NBD structure determined (1.6 Å), and was cocrystallized with ATP (but not Mg^{2+} or an equivalent cation) and so can be used to explore nucleotide-dependent

conformational changes. Although several NBDs have been crystallized as ''physiological'' dimers (Smith et al., 2002; Locher et al., 2002; Chen et al., 2003) we have chosen to initiate a systematic series of investigations by first characterizing the dynamic behavior of HisP, which has been crystallized in a monomeric state. Our simulations represent one of the first (Oloo and Tieleman, 2004) substantial studies of an ABC transporter NBD using MD, and so it is important to fully analyze both the strengths and limitations of this methodology using one of the simpler NBD systems.

A previous simulation study of HisP using MD has been published (Jones and George, 2002). However, this single simulation was of short duration (0.3 ns) relative to the likely timescale of protein conformational changes (>10 ns) and employed an approximate methodology whereby long-range electrostatic interactions were calculated using the ''cut-off'' method. In contrast we present the result of multiple simulations totaling 80 ns, in which HisP is simulated starting from a variety of configurations (no nucleotide, +ATP, +MgATP, etc.) to explore their influence on subsequent conformational dynamics. Furthermore, we have employed the particle mesh Ewald (PME) summation technique (Darden et al., 1993) that is generally acknowledged to provide a more accurate treatment of long-range electrostatic interactions than does a simple cutoff.

METHODS

The coordinates for HisP were obtained from the RCSB Protein Data Bank (www.rcsgb.org; entry 1B0U; Hung et al., 1998) without further alteration (except in simulations where nucleotide was removed). HisP simulation systems were generated by: i), solvation of the protein system using a preequilibrated box of SPC (Berweger et al., 1995) water molecules (the 379 crystal waters were retained in all simulations wherever possible); and ii), addition of random-positioned Na^+ and Cl^- ions equivalent to 0.1 M NaCl. In the simulation with bound Mg^{2+} (HisP5) the coordinates were obtained by fitting the ATP in HisP to the ATP in MJ0796 (PDB code 1L2T) (Smith et al., 2002). Then because MJ0796 was crystallized with NaATP, it was assumed that the position occupied by the Na ion would be the same for a Mg ion, so the Na coordinates were extracted. This was done by least-squares fitting the ATP molecules in MJ0796 and HisP (to give a root-mean-square deviation (RMSD) of 0.08 nm) and then adding the Na coordinates to the HisP file. The final box size was $8 \times 6 \times 7.5$ nm containing ~32,000 atoms (depending on the number of water molecules present). Default ionization states were used.

The system was then relaxed via 100 steps of steepest-descents energy minimization. After minimization, protein coordinates were restrained while allowing solvent molecules to relax their positions and optimize interactions with the proteins during a 50-ps simulation. During this equilibration nonhydrogen protein and ATP atoms were restrained harmonically using a force constant of 1000 kJ mol^{-1} nm^{-2}.

All simulations were performed in the NPT ensemble at 300 K. Electrostatics were calculated using particle mesh Ewald (Darden et al., 1993) with a 10-Å cutoff for the real space calculation. A cutoff of 10 Å was for van der Waals interactions. The temperatures of the protein and solvent (both water molecules and ions) were coupled separately, using the Berendsen thermostat (Berendsen et al., 1984) with a coupling constant of $\tau = 0.1$ ps. The pressure was coupled using the Berendsen algorithm at 1 bar with a coupling constant $\rho = 1$ ps, using a uniform compressibility of 4.5×10^{-5} bar^{-1}. The integration time step was 2 fs and coordinates were saved every 5 ps for subsequent analysis. The LINCS algorithm was used to restrain all bond lengths (Hess et al., 1997).

Simulations were run and analyzed using the GROMACS v3.0 (www.gromacs.org) molecular dynamics simulation package (Lindahl et al., 2001) with a modified GROMOS96 force field, parameter set ffG43a2, and/or locally written code. Secondary structure analysis used DSSP (Kabsch and Sander, 1983). Molecular graphics diagrams were generated using VMD (Humphrey et al., 1996) and PovRay (http://www.povray.org).

RESULTS

Simulations

Five simulations of the HisP monomers were run (summarized in Fig. 1 *C*). The two longer simulations (HisP1 and Hisp2; 30 ns each) were designed to investigate global conformational changes in response to bound ATP. In HisP1 the bound ATP was retained for the first 20 ns and then removed before a further 10-ns simulation. In simulation HisP2, the ATP was absent for the first 20 ns and then was returned to the binding site before the final 10-ns simulation (by least-squares fitting to the W_A motif and conserved tyrosine Y16 in the original ATP-bound PDB and extracting the coordinates for ATP). Much of our analysis and discussion will focus around these two simulations. Two shorter simulations (HisP3 and HisP4) were designed to explore in more detail specific interactions around the binding site identified in the longer simulations. A fifth simulation (HisP5) was run with MgATP bound in the active site in place of ATP to investigate the effects of the divalent cation on the interactions of protein and bound nucleotide.

ATP binding

Before discussion of conformational changes in HisP that reflect the presence of ATP in the nucleotide-binding pocket, we investigated whether ATP remains firmly bound in the pocket during the first phase (20 ns) of the HisP1 simulation and the second phase (10 ns) of the HisP2 simulation. This analysis was performed by calculating the distances between the conserved phosphate-binding residues in the W_A motif and the ATP phosphates. Specifically we calculated the distance between the centers of mass of Cα atoms of W_A residues 42–45 and the ATP phosphates. Additionally, we calculated the distance between the W_A lysine (Lys-45) and the β-phosphate. In all NBD structures crystallized to date, Lys-45 interacts with the β-phosphate of ATP, consistent with functional data demonstrating that this residue is involved with binding/hydrolysis of ATP. From the results of this analysis (Fig. 2) it is clear that in the HisP1 simulation, whose initial ATP-binding site configuration was as in the crystal structure (Hung et al., 1998), the ATP phosphates remain tightly bound (~0.45 nm) for the duration of the simulation because both the K45—β-phosphate and W_A Cα atoms—all phosphate distances remain near their starting values. In

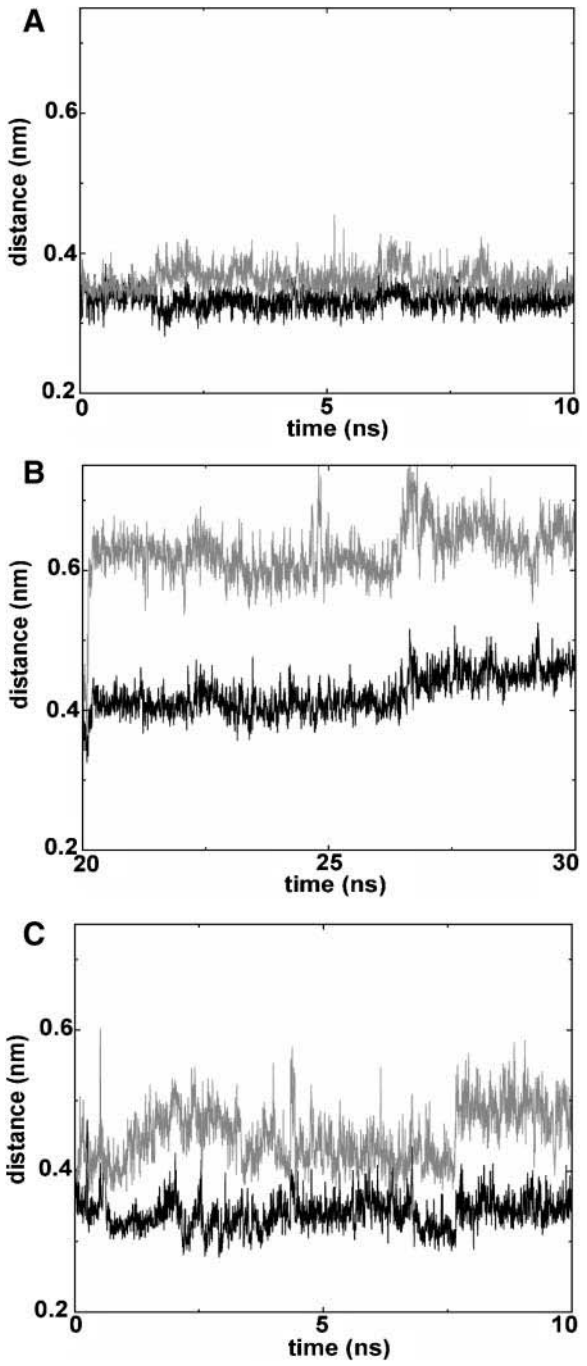

FIGURE 2 Analysis of ATP-phosphate/protein interactions during the: (*A*) HisP1 (0–10 ns), (*B*) HisP2 (20–30 ns), and (*C*) HisP5 (0–10 ns) simulations, showing the distance between the centers of mass of Lys-45 side-chain atoms to the ATP β-phosphate in black, and the Walker A Cα atoms (residues 42–45) to all of the ATP phosphate atoms in gray as functions of time.

contrast, in the HisP2 simulation (in which the ATP had been introduced into the binding site after first ''relaxing'' the protein for 20 ns in the absence of bound nucleotide), the ATP quickly (within ~0.2 ns) shifted to a more loosely bound state in which the close interactions between the β-phosphate and Lys-45 were completely lost. Further evidence suggesting that the protein-ATP interaction in the HisP2 simulation is reduced is that the distance between the other W_A residues and the ATP phosphates increases as a function of time and is significantly higher than in the HisP1 simulation. The plots for the HisP2 simulation demonstrate that some conformational changes occurred during the first 20 ns of simulation where ATP was absent. HisP5 presented an intermediate situation (Fig. 2 *C*) in that the β-phosphate/Lys-45 distance fluctuated between a reasonably close (~0.4 nm) and a looser (~0.5 nm) interaction during the 10-ns simulation. The remainder of the W_A residues were tightly bound to the ATP during the course of the simulation. The fact that the W_A—all phosphates distance is maintained but the Lys-45—β-phosphate distance is reduced reflects the fact the introduced divalent magnesium ion repels the positively charged lysine side chain.

Examination of the orientation of bound ATP at the $t = 0$ and 20 ns of the HisP1 simulation, and at $t = 20$ and 30 ns of the HisP2 simulation reveals some further differences (Fig. 3 *A*). In HisP1, although the close phosphate/W_A interaction is preserved, the adenosine group swings away from the binding site via rotation about the ribose–CH_2O-α-phosphate bonds (discussed below). A similar orientation was observed in HisP5 (not shown), in that the adenosine moiety swings out of the active site but the phosphates remain bound to the W_A motif. In contrast to HisP1, where the ATP undergoes a single conformational change, the adenosine group fluctuates between a number of conformational states indicated by the lack of smoothness in the RMSD plot (Fig. 4 *B*, *light gray line*). By contrast, in HisP2 the phosphate/W_A interaction is not maintained, but the adenine ring remains close to its initial location (Fig. 3 *B*).

In the HisP/ATP crystal structure the primary adenosine-active site interactions occur through: i), a water-mediated hydrogen bond between the OH group of a semiconserved tyrosine (Y16) and N7 of the adenine group; ii), hydrophobic

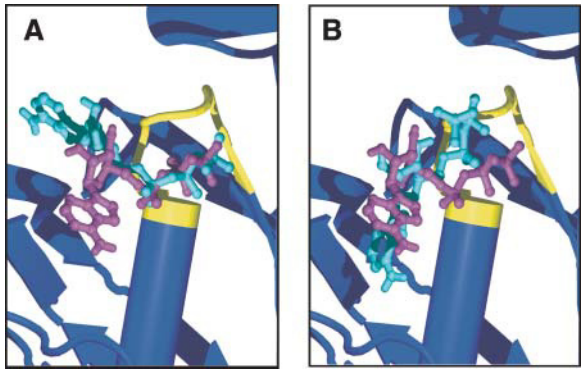

FIGURE 3 ATP/HisP interactions in the HisP1 and HisP2 simulations. (*A*) HisP1, the $t = 0$ ns (*purple*) and $t = 20$ ns (*cyan*) conformations of ATP; (*B*) HisP2, the $t = 20$ ns (*purple*) and $t = 30$ ns (*cyan*) conformations of ATP. The W_A motif (residues 42–45) is colored yellow. In both cases the protein is shown in the starting ($t = 0$ ns) configuration.

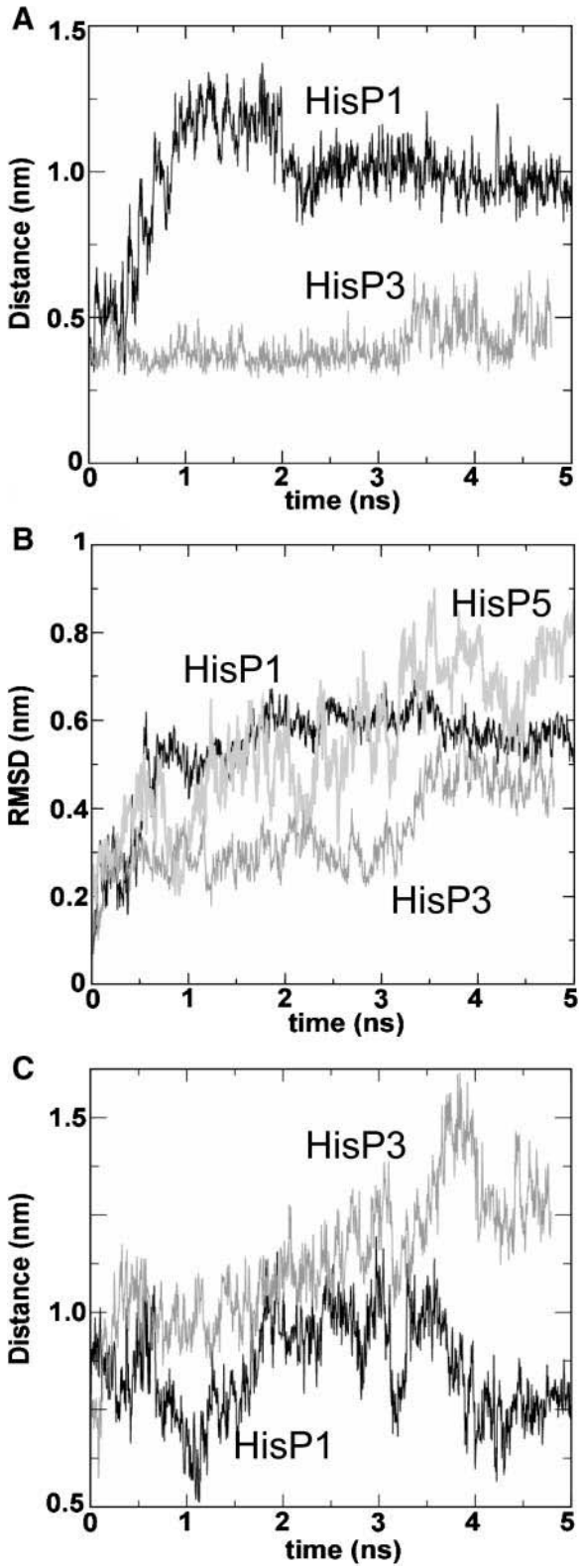

FIGURE 4 ATP-adenosine interactions. (*A*) The distance between the Y16 OH and the ATP N7 is shown as a function of simulation time for HisP1 (*black*) and HisP3 (*gray*). (*B*) The ATP all-atom RMSD (determined by fitting onto all Cα atoms in the protein, and calculating the RMSD of the ATP) is shown as a function of time for HisP1 (*black*), HisP3 (*gray*), and HisP5 (*light gray*). (*C*) The distance between the centers of mass of Q100 and the ATP γ-phosphate is shown as a function of simulation time for HisP1 (*black*) and HisP3 (*gray*) in panel *C*.

π-stacking interaction between the ring of Tyr-16 and adenine; and iii), a hydrogen bond between ND1 of H19 and the 2′ OH of adenosine. We investigated whether these interactions could be optimized thereby preventing the change in conformation of the ATP molecule observed during the HisP1 simulation. This was done via simulation HisP3, where the protein and ATP were restrained for 0.1 ns before free MD. After the restrained run, the system was checked to ensure that the water-mediated hydrogen bond between Tyr-16 OH and N7 of the adenine group was in an optimum geometry. This pretreatment of the MD system was indeed adequate to preserve the interaction between ATP and Tyr-16. This is shown by the time-dependent distance between the Tyr-16 OH and ATP N7 and further substantiated by RMSD versus time of the ATP molecule from its initial conformation for both the HisP1 and HisP3 simulations (Fig. 4). Interestingly, in simulation HisP5 (which is similar to HisP1 but with MgATP rather than ATP bound) some changes in the conformation of bound nucleotide still occur (Fig. 4 *B*), although (as will be discussed below) these do not result in the major changes in protein conformation observed in simulation HisP1. In both simulations HisP1 and HisP5, the interaction of the adenine ring of ATP with the conserved aromatic residue Tyr-16 is lost after ~1 ns of simulation time. However, interactions between the W_A residues and the ATP phosphate groups differ between the two simulations (see below).

Although the short restrained simulation (HisP3) does firmly ''lock'' the ATP in place for ~3 ns during the subsequent unrestrained simulation, further investigation suggested that this is perhaps not the most biologically meaningful simulation of monomeric HisP. This is exemplified by plots of the distance between the γ-phosphate of ATP and Q100, the conserved glutamine implicated in signal transduction (Karpowich et al., 2001; Urbatsch et al., 2000), which show that this interaction is perturbed in the HisP3 simulation (Fig. 4 *C*). Additionally, after 3ns during the HisP3 simulation the ATP molecule approaches a high RMSD state indicating that regardless of the initial treatment the ATP molecule will display high mobility. We therefore concluded that the unperturbed HisP1 simulation (starting directly from the crystal structure), in which the Q100-ATP contacts were retained, was a more biologically meaningful representation. This is supported by simulations (data not shown) of the monomeric (Karpowich et al., 2001) and dimeric MJ0796 (Smith et al., 2002) NBD structures, cocrystallized with ADP and ATP, respectively. These simulations show that the adenosine contact is lost in the monomeric simulation, but maintained in the dimeric simulation, demonstrating that the ''real'' contacts that lock the adenosine in the active site are

contributed from the signature sequence of the other NBD of the dimer.

Identification of the mobile domains

Having established that the ATP molecule remained bound to the active site during the first 20 ns of the HisP1 simulation, the ATP-induced conformational changes in HisP were investigated. To provide an initial insight into which regions of the protein undergo the largest motions, the root-mean squared fluctuations (RMSFs) of the Cα atoms from their initial positions were calculated for the different (i.e., with/without ATP) segments of the HisP1 and HisP2 simulations (Fig. 5). The RMSF plots show that both the Gln-loop and the α-helical subdomain (residues 109–171) exhibit an ATP-dependent mobility. This is evident from the fact that during the first 20 ns of the HisP1 simulation (i.e., while the ATP molecule was present) the α-helical subdomain and Q-loop displayed greater fluctuations than in both periods during which ATP was absent, i.e., the last 10 ns of the HisP1 simulation and the first 20 ns of the HisP2 simulation.

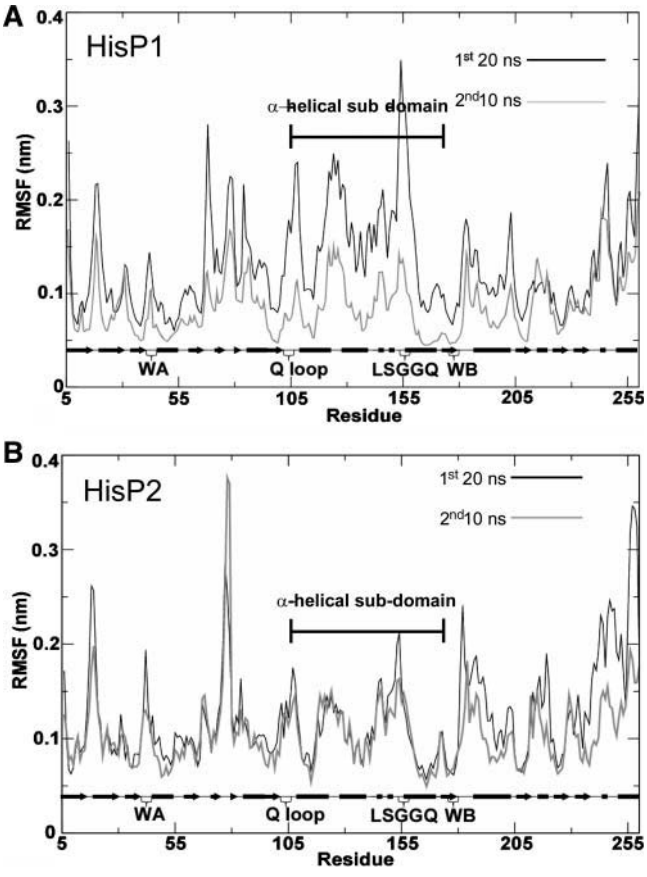

FIGURE 5 Conformational flexibility in HisP averaged over the MD simulations. The RMSF of the Cα atoms as a function of residue number are shown for the HisP1 (*A*) and HisP2 (*B*) simulations. The RMSF for the first phase of the simulations is shown as a black line, whereas that for the second phase is represented by a gray line. The secondary structure of the domain is indicated schematically above the residue number axis; helices are indicated by black boxes and strands by arrows. WA, Q loop, LSGGQ and WB denote the W_A motif, the Gln-loop, the signature sequence, and the W_B motif, respectively.

ATP-dependent mobility of the α-helical subdomain

The RMSF plots suggested that the α-helical subdomain had a greater mobility during the first-period (0–20 ns; with ATP present) HisP1 simulation. This was further investigated through calculation of time-dependent structural drift (measured as RMSDs of the Cα atoms from their initial coordinates), fitting the structures on different initial reference sets of coordinates to help dissect out the main conformational changes (Fig. 6). For HisP1 the RSMD of the α-helical subdomain fitted using all Cα atoms not in the α-helical subdomain shows a significant drift compared to that seen in either the RMSD of the entire NBD or of the α-helical subdomain when fitted upon itself. The low Cα RMSD of the α-helical subdomain fitted onto itself demonstrates that the drift of the subdomain is largely a rigid-body motion relative to the remainder of the NBD. No such drift in the α-helical subdomain RMSD was observed for the HisP2 simulation. In the HisP5 simulation an intermediate situation was observed, with some initial structural drift, but not as pronounced as in HisP1. In the HisP1 simulation, after the large drift of the α-helical subdomain at $\sim$4 ns, the removal of ATP at 20 ns does not trigger a relaxation back to the initial state. It is important to note that where conformational changes were observed, e.g., in HisP1, they occurred on a timescale of $\sim$10 ns and so would not be observed in substantially shorter simulations.

Rotation of the α-helical subdomain

The motion of the α-helical subdomain can be further characterized by plotting the angles made by the axes of each of the three main helices in the α-helical subdomain with respect to the axis of the third β-strand (β3) in the F1-type subdomain. Crystallographic analysis of prokaryotic ABC transporter NBDs in the presence and absence of nucleotide has suggested that an axis of rotation may exist in this region of the NBD structure (Karpowich et al., 2001; Smith et al., 2002; Yuan et al., 2001). It can be seen (Fig. 7 *A*) that in the HisP1 simulation at $\sim$4 ns (corresponding to the time at which the conformational shift of the α-helical subdomain is initiated) all three α-helices in the α-helical subdomain undergo a rotation relative to the β3 strand. No equivalent changes in helix angle (above the simulation ''noise'') were observed in the other HisP simulations (data not shown).

The rotations of component helices of the α-helical subdomain can be visualized by fitting the structure at $t = 20$ ns (i.e., at the end of the first phase of simulation HisP1) onto

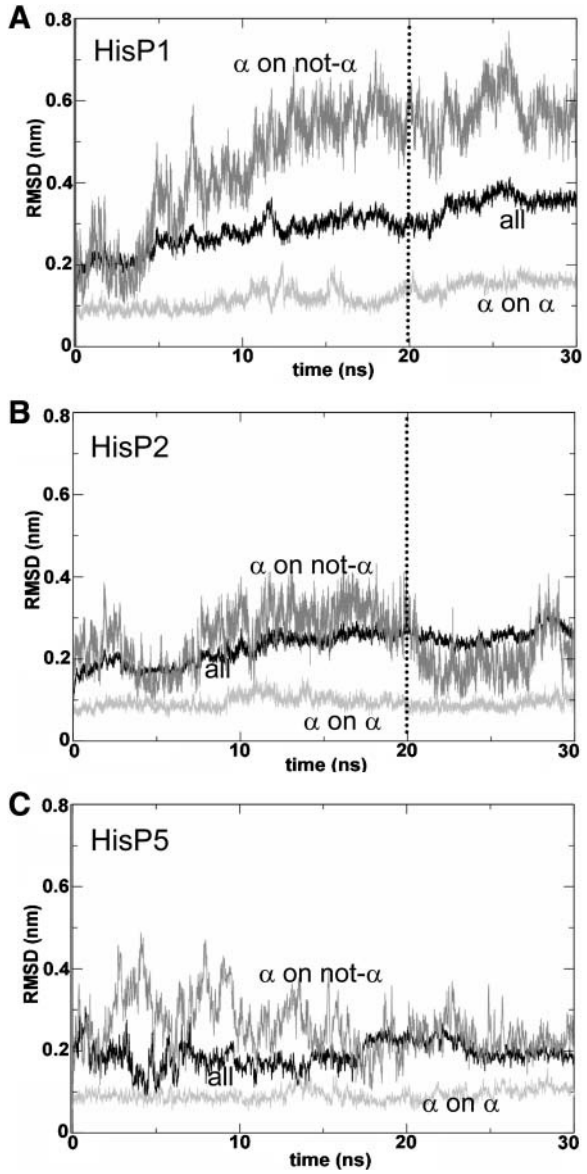

FIGURE 6 Conformational drift relative to the initial x-ray conformation during the HisP simulations. The Cα RMSDs are calculated for the HisP1 (*A*), HisP2 (*B*), and HisP5 (*C*) simulations. RMSDs for the entire HisP domain (*black*), for the α-helical subdomain fitted on all residues not in the α-helical subdomain (*dark gray*), and the α-helical subdomain fitted onto itself (*light gray*) are plotted as a function of the simulation time. The dashed line indicates the time at which ATP was removed (or added) in the HisP1 (or HisP2) simulations.

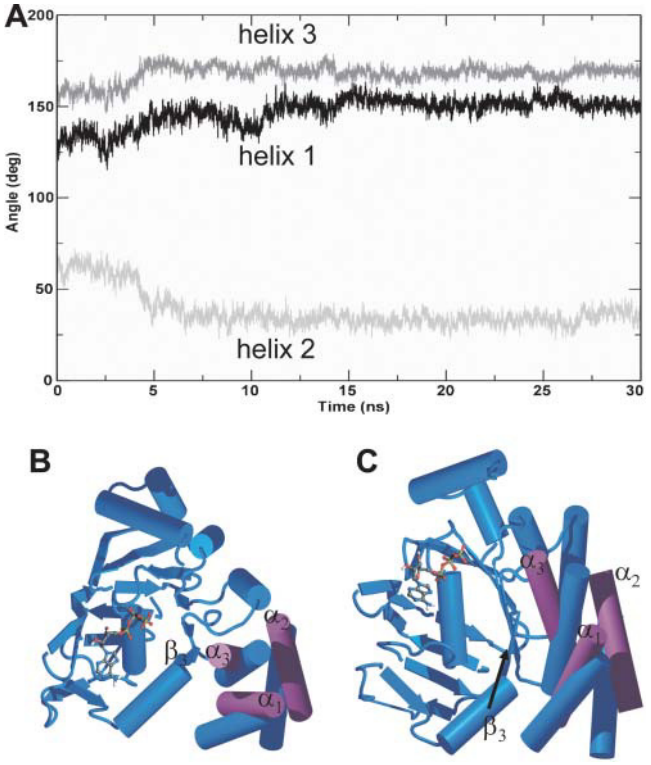

FIGURE 7 Rotational motion of the α-helical subdomain of HisP (residues 109–171). In panel *A* the angles of each of the three helices in the α-helical subdomain subtended to the F1-core subdomain were calculated by least-squares superposition of vectors corresponding to the helix axis and the β3-strand at 5-ps intervals throughout the simulations. Products of the resulting vectors were taken to derive the angle between β3 and individual α-helices. The angles for helix 1 (residues 110–120; *black*), helix 2 (residues 126–139; *dark gray*), and helix 3 (residues 156–170; *light gray*) are shown over the course of the HisP1 simulation. In panels *B* and *C*, two orthogonal views of the crystal structure of HisP (*blue*) and the structure derived after 20 ns of simulation in the presence of ATP (simulation HisP1; *magenta*) are shown. Structures were superimposed by least-squares fitting on residues not within the α-helical subdomain.

the initial conformation (Fig. 7, *B* and *C*). The rotations in the HisP1 simulation are characterized by an inwards pivoting of the helices toward the ATP-binding active site. The second helix rotates such that it becomes nearly parallel with β3.

Coupled movement of conserved sequence motifs

It is of interest to identify whether the conserved sequence motifs of ABC transporter NBDs undergo significant conformational changes during the simulations as this would increase our confidence in the functional relevance of such changes, e.g., for interdomain communication in the assembled transporter complex. Distances between sequence motifs (the signature sequence Gln-loop, His-loop, and the terminal polar residues of W_B) and the α-helix that terminates the W_A motif were calculated as a function of time (Fig. 8, *A* and *B*). The latter α-helix was selected as the marker from which the distances could be measured because: 1), it displayed low intradomain mobility in the RMSF analysis (Fig. 5); 2), it is structurally distinct from the four motifs under investigation; and 3), it could be used as a marker regardless of whether or not ATP is was present.

For the HisP1 simulation, of the measured distances, the signature sequence (see below) and the Gln-loop displayed noticeable changes in conformation. At ~4 ns, simultaneous with the α-helical subdomain rotation, the Gln-loop moves in transiently toward the active site and remains there for

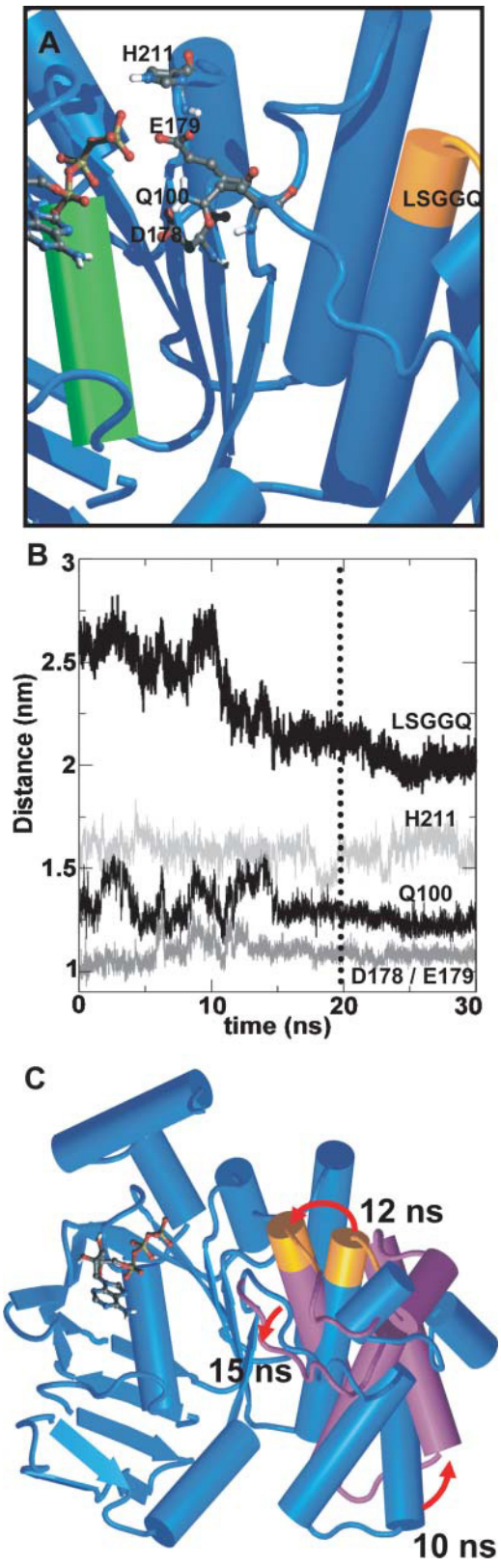

FIGURE 8 Identification of specific residue displacements in HisP during simulation HisP1. (*A*) The conserved residues at the ATP-binding site (Q100, D178, E179, H211; shown in CPK format), the signature sequence (LSGGQ; *yellow*) and the α-helix C-terminal to the W_A motif (residues 45–53; *green*) are highlighted. (*B*) Distances between the centers of mass of: i), the α-helix C-terminal to the W_A motif (residues 45–40) and ii), the conserved residues (Q100, D178, E179, H211) or the LSGGQ motif, are shown as functions of time. The vertical dotted line indicates the time at which ATP was removed from the simulation system. (*C*) The three distinct motions observed during HisP1 that suggest coupled movement are illustrated (*red arrows*). The first motion corresponds to the conclusion of the rotation/drift of the α-helical subdomain occurring at ~10 ns. After the conclusion of the α-helical subdomain motion the signature sequence shifts toward the ATP active site until ~12 ns, after which point it remains stable. The final motion is an inwards motion of the Q-loop that begins at the conclusion signature sequence motion and stabilizes at ~15 ns. Yellow indicates the conformation at $t = 20$ ns, i.e., after the motions are complete.

~2 ns, after which time it moves away again. After 15 ns the Gln-loop again pulls in toward the active site, a conformation that is maintained for the remainder of the simulation. The removal of the ATP molecule at 20 ns did not change the configuration of the loop.

The signature sequence also undergoes a significant displacement of ~0.5 nm in the HisP1 simulation compared with <0.1 nm and ~0.2 nm displacements in the HisP2 and HisP5 simulations, respectively (data not shown). The inward movement of the signature sequence in the HisP1 simulation commences at ~8 ns. Interestingly, this coincides with the conclusion of the rotation of the α-helices of the α-helical subdomain (at 7.5 ns). It is also worth noting that the conclusion of the signature sequence motion in turn coincides with the final inwards motion of the Q-loop, suggesting that some coupled motion exists between these domains (Fig. 8 *C*). This is in contrast to the W_B charged amino acids and the His-loop (the loop surrounding the conserved histidine His-211), which show little displacement from their starting conformation, presumably reflecting the continued coordination of nucleotide throughout the first 20-ns phase of the HisP1 simulation.

The coincidence in time of the motion of the Q-loop and of the rotation of the α-helical subdomain suggested that these two motions might be coupled, as previously proposed (Karpowich et al., 2001; Smith et al., 2002; Yuan et al., 2001). We therefore ran a simulation (HisP4) in which the Q-loop was restrained for 0.5 ns followed by 2.4 ns of unrestrained MD. We hypothesized that if we could force the Q-loop to remain in contact with the γ-phosphate of ATP then a rotation of the α-helical subdomain might be induced. In contrast to our hypothesis, although the 0.5 ns restrained run was sufficient to allow the Q-loop to remain in contact with the γ-phosphate, no simultaneous rotation of the α-helical subdomain was observed (not shown). This result suggests that other factors control the rotation of the α-helical subdomain.

Essential dynamics analysis of HisP1

To further dissect the motions underlying the ATP-induced conformational change of the α-helical subdomain observed in the HisP1 simulation, an essential dynamics analysis

(Amadei et al., 1993) of the simulated motions was preformed. The covariance matrix was constructed for the HisP1 simulation from the trajectory of the simulation between 2 and 20 ns. The eigenvector spectrum of the diagonalized covariance matrix indicates that the protein's main degrees of freedom are contained within the first 10 eigenvectors (the ''essential'' eigenvectors). In particular, ~40% of the observed motion is accounted for by the first eigenvector. Projecting the HisP1 simulation trajectory onto this eigenvector reveals that this principal motion of the protein indeed corresponds to rotation of the α-helical subdomain and an inwards motion of the signature sequence (Fig. 9 *A*).

Additional confirmation that the fluctuations of the α-helical subdomain are the most significant motions in the HisP1 simulation can be obtained by plotting the Cα displacements along the first and second eigenvectors (Fig. 9 *B*). For the first eigenvector the atomic displacement is highest in the α-helical subdomain, predominantly near the signature sequence. A concurrent high atomic displacement around the Q-loop indicates that there is some concerted motion between the Q-loop and signature sequence. We might further suspect that the high atomic displacement for the loop formed by residues 65–70 is coupled to the Q-loop/signature sequence motion, however, a detailed analysis of this peak revealed that it is not correlated to the motion within the α-helical subdomain. It instead results from the close proximity of residues 65–70 to the N-terminus of HisP.

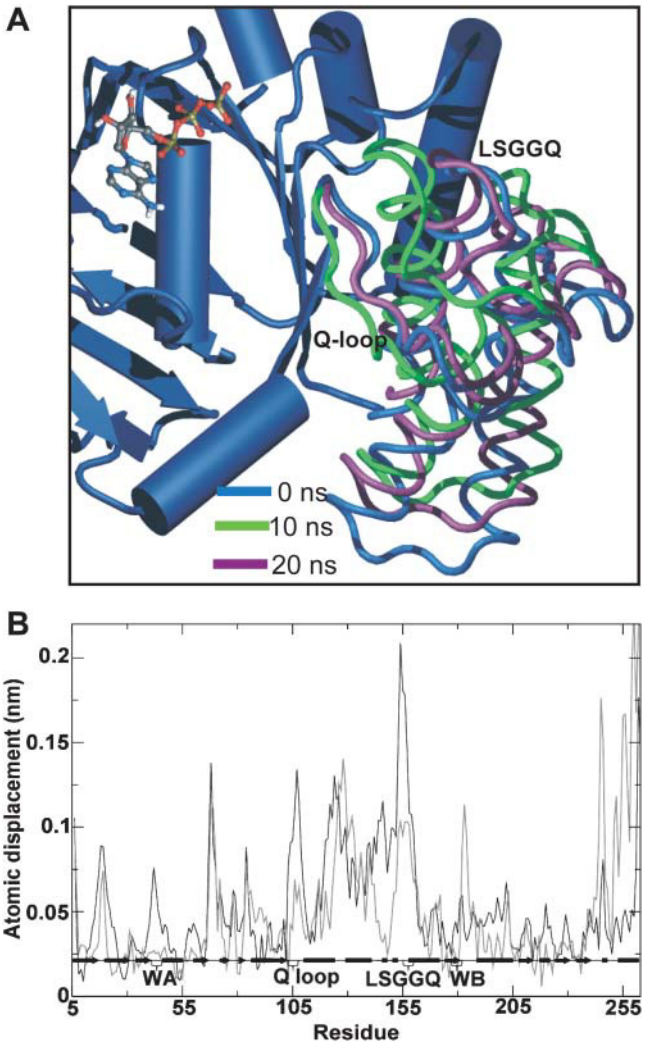

FIGURE 9 Essential dynamics analysis of the HisP1 simulation. (*A*) Motions corresponding to the principal eigenvector are illustrated by snapshots of the projected trajectory at $t = 0$ (*blue*), 3 (*magenta*), 6 (*yellow*), and 20 (*green*) ns. (*B*) Atomic displacements along the first (*black line*) and second (*gray line*) eigenvectors of the HisP1 simulation.

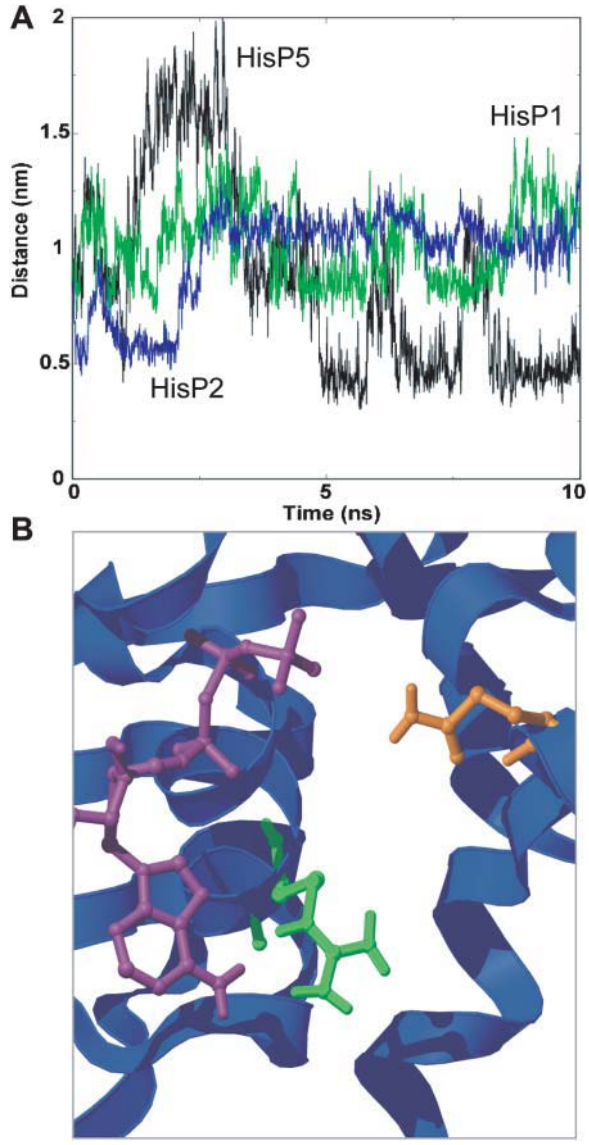

FIGURE 10 Interaction between Arg-50 and Q100. (*A*) The distance between the Arg-50 and Gln-100 side-chain atoms versus time for the first 10 ns of simulations HisP1 (*green*), HisP2 (*blue*), and HisP5 (*black*). In panel *B*, a snapshot of the binding site and relative locations of Arg-50 and Gln-100 is shown.

Simulation of HisP with MgATP versus ATP

Although the crystal structure of HisP corresponded to that in the presence of bound ATP, we have also investigated the conformational dynamics of the protein in the presence of bound MgATP (simulation HisP5), using the location of the Na^+ ion bound to ATP in the MJ0796 NBD dimer crystal structure (Smith et al., 2002) to position the Mg^{2+} ion relative to the ATP. The simulation stability of HisP5 was comparable to the other simulation systems (not shown). Interestingly a conformational change in the α-helical subdomain comparable to that in HisP1 was not detected. To characterize why the conformational change should take place in the absence of Mg, but not in the presence, we have tabulated the frequencies of interactions of residues around the binding site in both simulations (Table 1).

In Table 1 we have defined an interaction as being a distance <0.35 nm between a residue in the binding site and ATP. We have tabulated the interactions from three blocks in the simulations at 0–1ns, 5–6 ns, and 9–10 ns. We have counted interactions at 0.1-ns intervals in these blocks and thus the maximum number of interactions a given residue can have with ATP is 11.

A number of subtle differences are present between the interactions of residues near the binding site and ATP for the two simulations. In both simulations the interaction of ATP with the conserved aromatic residue Tyr-11 is lost after 1 ns in both the HisP1 and HisP5 simulations. Some interactions between the W_A residues that interact with the ATP phosphate groups (residues 40–47) are slightly different between the two simulations although the total number of interactions remains roughly the same. One dramatic difference in interactions between the two simulations is that between ATP and Arg-50. In the HisP1 simulation there is a strong interaction between ATP and Arg-50 throughout the 10 ns.

In contrast this interaction is immediately lost in the HisP5 simulation where Mg^{2+} was present and is not regained during the remainder of the simulation. We note that in the crystal structure of HisP, Arg-50 interacts with phosphate groups on the face of the ATP molecule to which Mg^{2+} was added in the HisP5 simulation. Thus in the presence of Mg^{2+} a favorable electrostatic interaction is lost (Fig. 10). We suggest that if Arg-50 is not interacting with ATP it is able to move more freely within the binding site and possibly interact with Gln-100. To test this, the distance between the Arg-50 and Gln-100 side-chain atoms was analyzed for the HisP1, HisP2, and HisP5 simulations (Fig. 10). Indeed, an interaction between Arg-50 and Gln-100 forms after 5 ns in the HisP5 simulation that is not present in the HisP1 simulation. We recall that the essential dynamics analysis of HisP1 demonstrated that the motions between the Gln-loop and the α-helical subdomain were correlated. Thus, if Gln-100 were prevented from rotating as occurs in the HisP5 simulation due to its interaction with Arg-50, this could inhibit a conformational change in the α-helical subdomain.

TABLE 1 Binding site comparison between ATP and MgATP simulations

Residue	0–1 ns	5–6 ns	9–10 ns
Interactions with ATP in HisP1 simulation			
Tyr-16	11	3	4
His-19	9	9	7
Glu-20	0	0	1
Val-21	2	1	3
Lys-23	0	2	5
Ser-41	11	6	6
Ser-43	0	7	4
Lys-45	10	11	11
Ser-46	9	7	9
Thr-47	11	11	11
Arg-50	8	8	10
Gln-228	8	5	9
Interactions with ATP in HisP5 simulation			
Arg-15	0	0	4
Tyr-16	11	0	0
His-19	6	9	0
Glu-20	0	0	6
Val-21	6	8	2
Lys-23	0	1	1
Ser-41	6	3	0
Ser-43	10	11	11
Lys-45	9	8	7
Ser-46	10	11	7
Thr-47	11	10	10
Arg-50	0	0	1
His-227	0	6	1
Gln-228	0	9	8

DISCUSSION

Understanding the conformational dynamics of proteins is a valuable complement to high-resolution structural information. We have employed relatively long (30 ns) MD simulations to investigate structural transitions of the ATP-hydrolyzing subunit (HisP) of a bacterial histidine transporter. We have compared simulations of HisP with ATP bound in the active site (as observed in the crystal structure), and without ATP bound. We have also compared the effects of ATP versus MgATP as a bound ligand. We have chosen to investigate the dynamics of HisP in the presence and absence of ATP (rather than comparing, e.g., ATP versus ADP) to analyze conformational dynamics events of nucleotide binding as opposed to nucleotide hydrolysis. In the catalytic cycle of an ABC transporter, the four main events at the NBD are: i), nucleotide binding; ii), nucleotide hydrolysis; iii), phosphate release; and iv), dissociation of ADP. Biochemical and kinetic data have demonstrated that hydrolysis and release of inorganic phosphate are likely to be rapid events in the catalytic cycle (Urbatsch et al., 1995). Thus, either nucleotide binding or ADP release must be a rate-limiting step. The binding of nucleotide to many ABC

transporters has been shown to be associated with conformational change. This has been demonstrated in intact transporters by virtue of altered proteolysis, immunoreactivity, and pharmacology (Mechetner et al., 1997; Martin et al., 2000; Sonveaux et al., 1999). More importantly in this study, conformational change in the isolated NBD subsequent to ATP binding has been demonstrated for both MalK and HisP (Kreimer et al., 2000; Schneider et al., 1994). Hence, our simulation analysis of events in an isolated NBD is a necessary and relevant first step toward understanding the catalytic cycle of complete ABC transporters.

Our MD analysis identifies conformational changes during the HisP1 simulation that could not be detected in HisP2 to HisP5 simulations. These changes are predominantly confined to the α-helical subdomain of HisP. Specifically we identify a rotation of three α-helices within the subdomain, and a movement of the signature sequence toward the bound nucleotide. In addition, we observed considerable conformational flexibility of the Q-loop, a region of the protein located at the interface between the α-helical and the F1-like subdomains. Throughout the HisP1 simulation, ATP remains tightly coordinated by the conserved residues of the W_A and W_B motifs.

Analysis of the HisP1 simulation suggests that the response to bound nucleotide involves conformational changes in the Q-loop. This was confirmed via simulation of HisP with bound MgATP in place of ATP. In this simulation (HisP5) the presence of Mg^{2+} allowed Arg-50 to contact Q100 thus restricting motions in the Q-loop. However, our attempts to induce a conformational change in HisP via manipulation of the Q-loop (simulation HisP4) suggest that other regions may play a role in triggering conformational change. It seems that after the conformational change in the α-helical subdomain, the signature loop enters a 6–7-ns period where it shows high conformational flexibility and a tendency to move ''inwards'' toward the nucleotide (although the distance to the nucleotide is still considerably >30 Å). As the signature motif adopts a conformation that it retains for the remainder of the simulation, the Q-loop undergoes another brief transition before remaining stable throughout the final 7 ns of the HisP1 simulation. Essential dynamics analysis of the principal eigenvector suggests that the motions of the Q-loop, α-helical subdomain, and signature sequence are correlated lending some evidence to our hypothesis of the steps involved in ATP binding at a single HisP NBD.

Recently, a relatively brief (0.39 ns) simulation of HisP has been presented (Jones and George, 2002). There are other methodological differences between this earlier simulation and that reported in this article. In the earlier study, a small water shell was used, along with treatment of long-range electrostatic interactions via a simple cutoff procedure. Our simulations are $\sim 80\times$ longer and employ a more standard simulation methodology, including periodic boundary conditions and treatment of long-range electrostatics via PME (Darden et al., 1993). Our simulations demonstrate that conformational changes still occur in the protein after $\sim$15 ns (and it is likely that equilibrium has not been fully reached in 20 ns). However, despite these differences it is encouraging to observe some similarities in conclusions from the two studies, in particular the suggestion that the α-helical domain is important in the transmission of conformational changes to the TMDs (Jones and George, 2002). This suggests some aspects of the simulation results may be relatively robust to the exact methodologies employed.

Extrapolation to the functionally important dynamics of the intact transporter is made more difficult as the simulations are based on monomeric HisP. It is clear that ABC transporter NBDs in vivo function as a dimer (Kerr, 2002). Crystallographic studies of the vitamin B_{12} importer BtuCD (from *Escherichia coli*; PDB code 1L7V), the branched-chain amino acid transporter MJ0796 (from *Methanococcus jannaschii*; PDB code 1L2T), and the maltose transporter NBDs MalK (from *E. coli*; PDB codes 1Q12, 1Q1B, 1Q1E) indicate a physiologically relevant mode of packing for the NBD dimer (Locher et al., 2002; Smith et al., 2002; Chen et al., 2003) (although we note that some possible complications are raised via comparisons with the crystal structures of MsbA; Chang and Roth, 2001; Chang, 2003; Campbell et al., 2003). In this context we attempted to model the HisP NBD dimer by fitting two HisP molecules onto dimeric MJ0796 (data not shown). Interestingly, despite the fact that both HisP and the MJ0796 dimer were cocrystallized with ATP, and that the two species of NBD share considerable sequence identity ($>$40%), a large number of steric conflicts resulted from the fitting procedure. It should be noted that many of the same steric conflicts are introduced by fitting the monomeric MJ0796 x-ray structure (Yuan et al., 2001) onto the dimer (Smith et al., 2002). Thus, further studies will be required to model the possible conformational changes of HisP upon dimerization.

Despite the possible limitations of our study, the observation that the Arg-50–Gln-100 interaction prevents rotation of the α-helical subdomain does present an intriguing hypothesis of how MgATP binds. It is clear that Mg^{2+} is not required for binding of nucleotide to the NBDs, and that its presence is largely required for hydrolysis (Hung et al., 1998). It seems possible Mg^{2+} may modulate the interaction of Arg-50 with ATP and thus may modulate the rotation of the α-helical subdomain. This prediction should be amenable to experimental evaluation. In addition to this specific proposal, we have demonstrated that nucleotide-induced conformational changes are amenable to current MD techniques. In particular, we have shown that the timescales currently accessible in MD simulations are sufficient to reveal the initial motion of the α-helical subdomain of the HisP NBD induced by bound nucleotide.

Our special thanks to Alessandro Grottesi and Phil Biggin for stimulating discussions.

J.D.C. is supported by a Wellcome Trust Structural Biology Studentship and thanks Linacre College for a Canadian National Scholarship. I.D.K. was supported by a Wellcome Trust Research Career Development Fellowship. M.S.P.S. thanks both the Wellcome Trust and the Biotechnology and Biological Sciences Research Council for their continued financial support and the Oxford Supercomputing Centre for access to resources.

REFERENCES

Amadei, A., A. B. M. Linssen, and H. J. C. Berendsen. 1993. Essential dynamics of proteins. *Proteins*. 17:412–425.

Arinaminpathy, Y., M. S. P. Sansom, and P. C. Biggin. 2002. Molecular dynamics simulations of the ligand binding domain of the ionotropic glutamate receptor, GluR2. *Biophys. J*. 82:676–683.

Berendsen, H. J. C., J. P. M. Postma, W. F. van Gunsteren, A. DiNola, and J. R. Haak. 1984. Molecular dynamics with coupling to an external bath. *J. Chem. Phys*. 81:3684–3690.

Berweger, C. D., W. F. van Gunsteren, and F. Mullerplathe. 1995. Force-field parameterization by weak-coupling: reengineering SPC water. *Chem. Phys. Lett*. 232:429–436.

Bockmann, R. A., and H. Grubmuller. 2002. Nanoseconds molecular dynamics simulation of primary mechanical energy transfer steps in F1-ATP synthase. *Nat. Struct. Biol*. 9:198–202.

Campbell, J. D., P. C. Biggin, M. Baaden, and M. S. P. Sansom. 2003. Extending the structure of an ABC transporter to atomic resolution: modelling and simulation studies of MsbA. *Biochemistry*. 42:3666–3673.

Chang, G. 2003. Structure of MsbA from *Vibrio cholera*: a multidrug resistance ABC transporter homolog in a closed conformation. *J. Mol. Biol*. 330:419–430.

Chang, G., and C. B. Roth. 2001. Structure of MsbA from E. coli: a homolog of the multidrug resistance ATP binding cassette (ABC) transporters. *Science*. 293:1793–1800.

Chen, J., G. Lu, J. Lin, A. L. Davidson, and F. A. Quiocho. 2003. A tweezers-like motion of the ATP-binding cassette dimer in an ABC transport cycle. *Mol. Cell*. 12:651–661.

Darden, T., D. York, and L. Pedersen. 1993. Particle mesh Ewald: an N.log(N) method for Ewald sums in large systems. *J. Chem. Phys*. 98:10089–10092.

Davidson, A. L., S. S. Laghaeian, and D. E. Mannering. 1996. The maltose transport system of Escherichia coli displays positive cooperativity in ATP hydrolysis. *J. Biol. Chem*. 271:4858–4863.

Diederichs, K., J. Diez, G. Greller, C. Muller, J. Breed, C. Schnell, C. Vonrhein, W. Boos, and W. Welte. 2000. Crystal structure of MalK, the ATPase subunit of the trehalose/maltose ABC transporter of the archaeon *Thermococcus litoralis*. *EMBO J*. 19:5951–5961.

Druley, T. E., W. D. Stein, and I. B. Roninson. 2001. Analysis of MDR1 P-glycoprotein conformational changes in permeabilized cells using differential immunoreactivity. *Biochemistry*. 40:4312–4322.

Efremov, R. G., Y. A. Kosinsky, D. E. Nolde, R. Tsivkovskii, A. S. Arseniev, and S. Lutsenko. 2004. Molecular modelling of the nucleotide-binding domain of Wilson's disease protein: location of the ATP-binding site, domain dynamics and potential effects of the major disease mutations. *Biochem. J*. 382:293–305.

Fetsch, E. E., and A. L. Davidson. 2002. Vanadate-catalyzed photocleavage of the signature motif of an ATP-binding cassette (ABC) transporter. *Proc. Natl. Acad. Sci. USA*. 99:9685–9690.

Hess, B., H. Bekker, H. J. C. Berendsen, and J. G. E. M. Fraaije. 1997. LINCS: a linear constraint solver for molecular simulations. *J. Comput. Chem*. 18:1463–1472.

Higgins, C. F. 1992. ABC transporters: from microorganisms to man. *Annu. Rev. Cell Biol*. 8:67–113.

Higgins, C. F., P. D. Haag, K. Nikaido, F. Ardeshir, G. Garcia, and G. F. Ames. 1982. Complete nucleotide-sequence and identification of membrane-components of the histidine transport operon of *S. typhimurium*. *Nature*. 298:723–727.

Holland, I. B., and M. A. Blight. 1999. ABC-ATPases, adaptable energy generators fuelling transmembrane movement of a variety of molecules in organisms from bacteria to humans. *J. Mol. Biol*. 293:381–399.

Humphrey, W., A. Dalke, and K. Schulten. 1996. VMD: visual molecular dynamics. *J. Mol. Graph*. 14:33–38.

Hung, L. W., I. X. Y. Wang, K. Nikaido, P. Q. Liu, G. F. L. Ames, and S. H. Kim. 1998. Crystal structure of the ATP-binding subunit of an ABC transporter. *Nature*. 396:703–707.

Jones, P. M., and A. M. George. 2002. Mechanism of ABC transporters: a molecular dynamics simulation of a well characterized nucleotide-binding subunit. *Proc. Natl. Acad. Sci. USA*. 99:12639–12644.

Jones, P. M., and A. M. George. 2004. The ABC transporter structure and mechanism: perspectives on recent research. *Cell. Mol. Life Sci*. 61:682–699.

Kabsch, W., and C. Sander. 1983. Dictionary of protein secondary structure: pattern-recognition of hydrogen-bonded and geometrical features. *Biopolymers*. 22:2577–2637.

Karpowich, N., O. Martsinkevich, L. Millen, Y. R. Yuan, P. L. Dai, K. MacVey, P. J. Thomas, and J. F. Hunt. 2001. Crystal structures of the MJ1267 ATP binding cassette reveal an induced-fit effect at the ATPase active site of an ABC transporter. *Structure*. 9:571–586.

Kerr, I. D. 2002. Structure and association of ATP-binding cassette transporter nucleotide-binding domains. *Biochim. Biophys. Acta*. 1561: 47–64.

Kreimer, D. I., K. P. Chai, and G. F. L. Ames. 2000. Nonequivalence of the nucleotide-binding subunits of an ABC transporter, the histidine permease, and conformational changes in the membrane complex. *Biochemistry*. 39:14183–14195.

Lindahl, E., B. Hess, and D. van der Spoel. 2001. GROMACS 3.0: a package for molecular simulation and trajectory analysis. *J. Mol. Model*. 7:306–317.

Linton, K. J., and C. F. Higgins. 1998. The Escherichia coli ATP-binding cassette (ABC) proteins. *Mol. Microbiol*. 28:5–13.

Linton, K. J., and C. F. Higgins. 2002. P-glycoprotein misfolds in Escherichia coli: evidence against alternating-topology models of the transport cycle. *Mol. Membr. Biol*. 19:51–58.

Locher, K. P., A. T. Lee, and D. C. Rees. 2002. The *E. coli* BtuCD structure: a framework for ABC transporter architecture and mechanism. *Science*. 296:1091–1098.

Loo, T. W., M. C. Bartlett, and D. M. Clarke. 2002. The ''LSGGQ'' motif in each nucleotide-binding domain of human p-glycoprotein is adjacent to the opposing Walker A sequence. *J. Biol. Chem*. 277:41303–41306.

Martin, C., G. Berridge, P. Mistry, C. Higgins, P. Charlton, and R. Callaghan. 2000. Drug binding sites on P-glycoprotein are altered by ATP binding prior to nucleotide hydrolysis. *Biochemistry*. 39:11901–11906.

Mechetner, E. B., B. Schott, B. S. Morse, W. D. Stein, T. Druley, K. A. Davis, T. Tsuruo, and I. B. Roninson. 1997. P-glycoprotein function involves conformational transitions detectable by differential immunoreactivity. *Proc. Natl. Acad. Sci. USA*. 94:12908–12913.

Morbach, S., S. Tebbe, and E. Schneider. 1993. The ATP-binding cassette (ABC) transporter for maltose maltodextrins of Salmonella typhimurium: characterization of the ATPase activity associated with the purified MalK subunit. *J. Biol. Chem*. 268:18617–18621.

Nikaido, K., and G. F. L. Ames. 1999. One intact ATP-binding subunit is sufficient to support ATP hydrolysis and translocation in an ABC transporter, the histidine permease. *J. Biol. Chem*. 274:26727–26735.

Okimoto, N., K. Yamanaka, A. Suenaga, M. Hata, and T. Hoshino. 2002. Computational studies on prion proteins: effect of Ala117→Val mutation. *Biophys. J*. 82:2746–2757.

Okimoto, N., K. Yamanaka, J. Ueno, M. Hata, T. Hoshino, and M. Tsuda. 2001. Theoretical studies of the ATP hydrolysis mechanism of myosin. *Biophys. J.* 81:2786–2794.

Oloo, E. O., and D. P. Tieleman. 2004. Conformational transitions induced by the binding of mgATP to the vitamin B12 ATP-binding cassette (ABC) transporter BtuCD. *J. Biol. Chem.* 279:45013–45019.

Pang, A., Y. Arinaminpathy, M. S. P. Sansom, and P. C. Biggin. 2003. Interdomain dynamics and ligand binding: molecular dynamics simulations of glutamine binding protein. *FEBS Lett.* 550:168–174.

Rinaldo, D., and M. J. Field. 2003. A computational study of the open and closed forms of the N-lobe human serum transferrin apoprotein. *Biophys. J.* 85:3485–3501.

Rosenberg, M. F., G. Velarde, R. C. Ford, C. Martin, G. Berridge, I. D. Kerr, R. Callaghan, A. Schmidlin, C. Wooding, K. J. Linton, and C. F. Higgins. 2001. Repacking of the transmembrane domains of P-glycoprotein during the transport ATPase cycle. *EMBO J.* 20:5615–5625.

Schneider, E., S. Wilken, and R. Schmid. 1994. Nucleotide-induced conformational-changes of MalK, a bacterial ATP binding cassette transporter protein. *J. Biol. Chem.* 269:20456–20461.

Sharom, F. J. 2003. Probing of conformational changes, catalytic cycle and ABC transporter function. *In* ABC Proteins: From Bacteria to Man. B. I. Holland, S. P. C. Cole, K. Kuchler, and C. F. Higgins, editors. Academic Press, London, UK.

Smith, P. C., N. Karpowich, L. Millen, J. E. Moody, J. Rosen, P. J. Thomas, and J. F. Hunt. 2002. ATP binding to the motor domain from an ABC transporter drives formation of a nucleotide sandwich dimer. *Mol. Cell.* 10:139–149.

Sonveaux, N., A. B. Shapiro, C. Vigano, and J. M. Ruysschaert. 1999. Ligand-mediated structure changes of reconstituted P-glycoprotein. *Biophys. J.* 76:102. (Abstr.).

Urbatsch, I. L., K. Gimi, S. Wilke-Mounts, and A. E. Senior. 2000. Investigation of the role of glutamine-471 and glutamine-1114 in the two catalytic sites of P-glycoprotein. *Biochemistry.* 39:11921–11927.

Urbatsch, I. L., B. Sankaran, S. Bhagat, and A. E. Senior. 1995. Both P-glycoprotein nucleotide-binding sites are catalytically active. *J. Biol. Chem.* 270:26956–26961.

Walker, J. E., M. Saraste, M. J. Runswick, and N. J. Gay. 1982. Distantly related sequences in the alpha-subunits and beta-subunits of ATP synthase, myosin, kinases and other ATP-requiring enzymes and a common nucleotide binding fold. *EMBO J.* 1:945–951.

Yuan, Y. R., S. Blecker, O. Martsinkevich, L. Millen, P. J. Thomas, and J. F. Hunt. 2001. The crystal structure of the MJ0796 ATP-binding cassette: implications for the structural consequences of ATP hydrolysis in the active site of an ABC transporter. *J. Biol. Chem.* 276:32313–32321.